A Model of a Fundamental-mode Lorentz Force Actuated Flexural Plate Wave Resonator

by

Misha K. Hill

Submitted to the Department of Electrical Engineering and

Computer Science in partial fulfillment of the requirements for the degree of

Master of Engineering in Electrical Engineering and Computer Science

at the Massachusetts Institute of Technology

May 11, 1999

[Some pgs]

Signature of Author _____
Department of Electrical Engineering and Computer Science
May 11, 1999

Certified by _____
Stephen D. Senturia, Barton L. Weller Professor
Department of Electrical Engineering and Computer Science
Thesis Supervisor

Accepted by _____
Arthur C. Smith
Chairman, Department Committee on Graduate Theses
Department of Electrical Engineering and Computer Science

A Model of a Fundamental-mode
Lorentz Force Actuated Flexural Plate Wave Resonator
by
Misha K. Hill

Submitted to the
Department of Electrical Engineering and Computer Science

May 11, 1999

In partial fulfillment of the requirements for the degree of
Master of Engineering in Electrical Engineering and Computer Science

ABSTRACT

The flexural plate wave resonator provides a potentially useful sensor platform. Lorentz force actuated devices that resonate in the fundamental mode have been developed at Sandia National Laboratories. These devices demonstrate unexpected variability in such attributes as resonant frequency and response quality. This thesis provides a lumped element model of the device that allows incorporation into control electronics and explains the observed data. Finite element and analytic models of the device explain the variability and provide the values used in the lumped element model as well as a means for detailed analysis of device behavior. Data collected at Sandia verify the accuracy of these models. Analysis of the experimental data using these models indicates areas for improvement in device design and testing. Such models and the tools used to create them are critical to efficient MEMS device design, allowing understanding of and improvement in device function without costly prototype production.

Thesis Supervisor: Stephen D. Senturia
Title: Barton L. Weller Professor, Department of Electrical Engineering and Computer Science

Acknowledgments

I would like to take this opportunity to thank the many individuals who have contributed to my personal and academic growth culminating in the completion of this thesis.

Most important in this respect has been the expert guidance of my research advisor Stephen Senturia. He has taught me to see the patterns in data and to make use of these to find what I am looking for. I thank Steve for this and for giving me the opportunity to work in this field both technically and financially. I also thank Steve Martin, Mike Butler, and Kent Schubert at Sandia National Labs for their support of my interests, providing me the opportunity to use their facilities, guiding me in my research, and financially supporting my work at MIT.

The members of my research group in the Microsystems Technologies Laboratories have been invaluable in making this work a success. Mat Varghese, Erik Deutsch, Alicia Volpicelli, and Jan Mehner helped me to make use of the resources I needed and taught me what I needed to know about modeling and simulation. Additionally, Bart Romanowich and Vladamir Rabinowich of Microcosm technologies were of great help, giving their time to make sure I had the tools I needed.

Thanks also to Robert Waldschmidt, Au-Shyang Chu, and Robert Sanchez, of the Sandia National Labs Microsensor Research and Development department, who helped me with my experiments and data collection during my time at Sandia.

Finally, I thank my parents and sister for their love, support and guidance throughout my life, trusting my decisions and always being there for me when I needed them.

This work was supported in part by DARPA under contract J-FB1-95-215 and by the Sandia National Laboratories.

Table of Contents

List of figures

1 Introduction

1.1 Flexural Plate Wave devices

Surface acoustic wave (SAW) devices are well established as an effective sensor platform [1]. The flexural plate wave (FPW) device is a variation of the SAW in which the acoustic substrate is thin enough that the bending stiffness becomes negligible and the device exhibits membrane behavior, in which case the wave deforms the shape of the entire substrate. Unlike SAW devices, wave frequency in the membrane decreases with density in FPW devices, making them effective for sensing mass loading at low frequencies. They also are greatly affected by the stress in the membrane, so such factors as temperature and pressure loading affect their behavior. The original FPW devices described by White and Wenzel use piezoelectric materials to excite and detect a propagating acoustic wave [2]. These devices have been used as such things as chemical vapor sensors, biosensors, and acoustic pumps [3, 4 5], and are marketed by a number of companies, including Berkeley Microsensors, founded by White and Wenzel.

1.2 Magnetically excited FPW

More recently, researchers at Sandia National Laboratories (SNL) have modified the FPW device. By using Lorentz forces to excite and detect the wave, their magnetically excited FPW (mag-FPW) resonator avoids piezoelectric materials, allowing it to be fabricated in a standard Si processing lab and to be integrated with Si based control electronics [6]. Additionally, these FPW devices operate as the resonant element of an oscillator. The frequency of the oscillator is affected by the environmental factors that one might wish to sense. Use of these devices as pressure sensors [7] and strain gages [8] has been demonstrated, and other applications are being investigated.

The original mag-FPW resonators were designed with gold or aluminum meander line transducers (MLT) positioned over anti-nodes of a selected eigenmode of the membrane. An alternating current passing through the MLT while in presence of an in-plane magnetic field from external magnets results in Lorentz forces exciting the selected resonant mode (figure 1). In the two-port version of these devices, one MLT activates the resonant mode and a second one detects it. In the one-port version, only one MLT is present, used both to activate and detect the resonance. In both cases the resonance is detected through the impedance due to the back-emf resulting from motion of the conductor through the magnetic field.

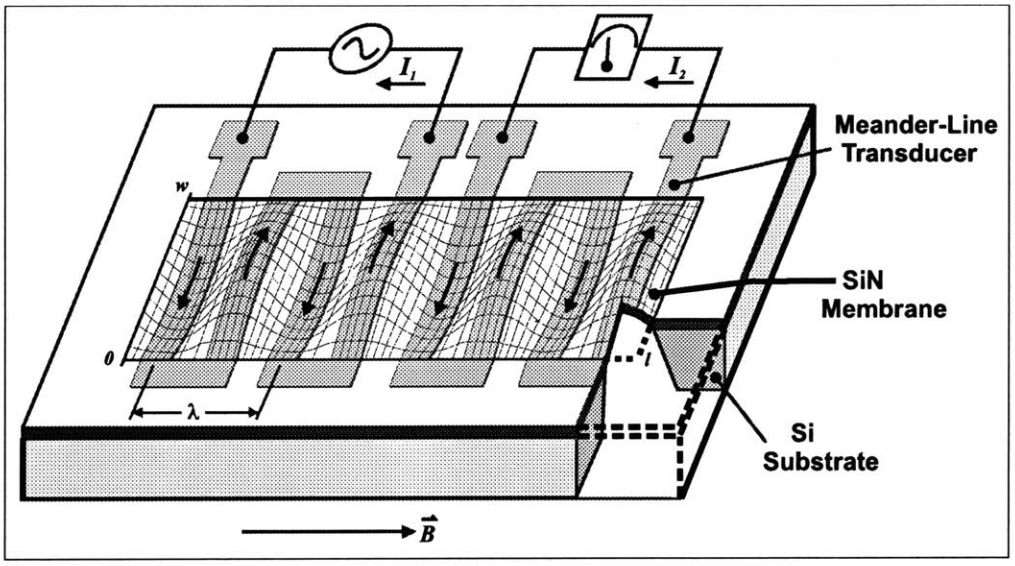

Figure 1 - Schematic of magnetically excited FPW resonator

1.3 Fundamental-mode mag-FPW

The inventors of the mag-FPW have developed a fundamental-mode version of the device, in which the transducer lines carry current in a uniform direction across a circular membrane, exciting only the first harmonic mode. I had the opportunity in the summer of 1998 to work on these devices at Sandia, observing their behavior and response to a

variety of environmental factors. It is the purpose of this thesis to provide a model that will explain those observations and allow further development of this sensor platform.

The fundamental-mode devices were fabricated in three sizes, 1, 2, and 3 mm in diameter. The first lot of devices, on which the most data is available, were made using a 0.5 μm thick SiN layer as the membrane. The wafers were supplied to Sandia from MCNC with the silicon-nitride layer already deposited. Deposition and patterning of the aluminum transducer and etching of the wafer to release the membrane was performed at the Micro-Development Lab at Sandia. Later devices were made from wafers with 1 μm nitride layers from Strataglass and 2 μm nitrides deposited at Stanford University but little information is available about the performance of these devices. More recently, they have begun fabricating mag-FPW resonators using amorphous diamond films for the membranes. These can be grown on-site, avoiding the use of third party sources [9]. All of these devices operate in the ultrasonic frequency ranges of 60-300 kHz. Due to the details of the etch processes used to fabricate the early devices, there is a fair amount of variability in the effective diameters of the membranes, and hence variability in their response to environmental factors. The fabrication process is described in detail in Appendix A.

2 Data

2.1 Background

During the summer of 1998, I worked at Sandia National Laboratories as a student intern. The fundamental-mode mag-FPW had just been developed at that time and had not been extensively studied. With the expectation that upon returning to MIT in the fall I would create a model to predict the behavior of these devices, I was assigned the task of studying the devices and generating as much information as possible to assist in the verification of the model. I designed a series of experiments to collect data about the behavior of the devices and the effect various environmental factors would have on their performance. In the beginning, only a portion of the lot 1 devices were available for testing. Later in the summer, devices from the second wafer of lot 1 became available.

2.2 Experimental Setup

2.2.1 Test setup

The main set of experiments concerned the resonant frequency and frequency response of the devices under various environmental factors. The device under test was attached to a custom designed printed circuit board. Although some devices had already been attached to boards using a cyano-acrilate glue around the perimeter of the die, those I worked on were attached only at one corner of the die using an epoxy that would hold better and not add stress to the device. The contact pads of the transducer were sonically wire-bonded to the conductors on the PC board using gold ribbon. The PC board was then placed inside a brass fixture that would allow control of the ambient gas (figure 2). Connections between the board and the coaxial connectors on the fixture were originally made using jumpers and later with direct soldering. The board was initially left floating

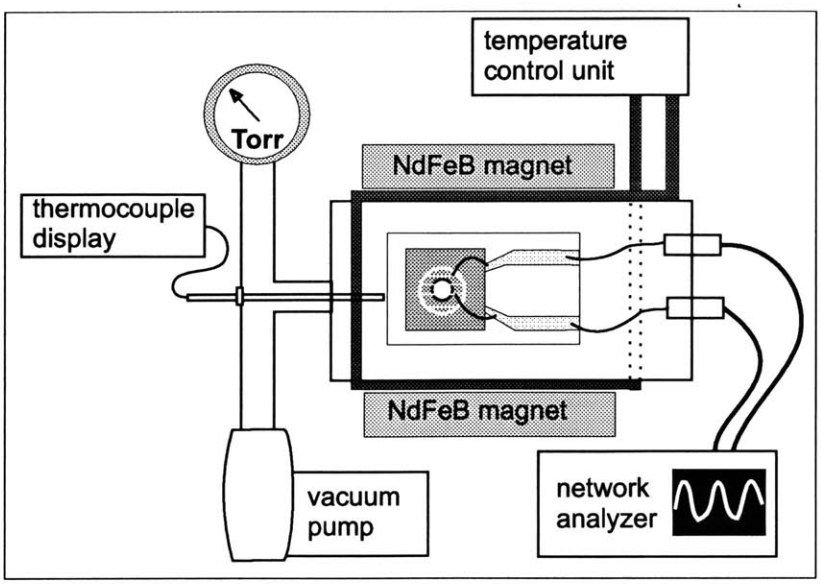

Figure 2 - Test setup for frequency response measurements

inside the fixture, held in place only by the electrical connections. In later experiments, it was attached to the fixture using small bolts to ensure proper grounding and prevent motion of the board. The content and pressure of the ambient gas inside the fixture were controlled with a vacuum pump and measured using a Convectron pressure gage. The temperature of the fixture was controlled by pumping a temperature-controlled solution of water and ethylene-glycol though copper tubes soldered to the outside of the fixture. Temperature on the surface of the fixture was monitored using a K-type thermocouple placed inside a copper tube soldered to the surface of the fixture in the same manner as the temperature-control tubes. For later experiments a, J-type thermocouple was inserted directly into the fixture through a pass-through in the vacuum pump tubing. This allowed direct monitoring of the temperature of the ambient gas. Large NdFeB magnets (5 cm square) were placed on either side of the brass fixture and held in place with an iron C-clamp. This clamp was intended both to hold the magnets in place and to contain the

B-field. This arrangement resulted in a magnetic field at the position of the resonator of about 2 kG. In an actual sensor application, smaller magnets would be placed directly adjacent to the sensor, but that could not be done with the fixture used here. With the distance between the magnets required by this fixture, the large magnets were necessary to achieve a magnetic field of sufficient strength at the sensor. The coaxial connectors of the fixture were connected to an HP 8751a network analyzer.

2.2.2 Pressure & power consideration

After placing a device in the test fixture, pressure was lowered to the range in which device response could be observed. Due to the low power output of the network analyzer, these tests had to be conducted at pressures below roughly 1 Torr. At higher pressures, the signal would be lost in the noise. At low pressures, the low power available was sufficient to produce observable signals, though they were noisy. Raising the power toward the analyzer's limit improved the signal to noise ratio, but sometimes caused the resonator to exhibit nonlinear, or Duffing spring, behavior. An example plot of this effect is shown in figure 3. Raising the pressure restored linear behavior but diminished the magnitude of the response. In each test, a compromise had to be made between pressure and power to optimize signal strength and noise while maintaining linearity in the mechanical behavior.

2.2.3 Resonant Frequency

2.2.3.1 Experiment

The first set of data collected in this experiment concerned the resonant frequency of the device, the main attribute likely to be used in sensing applications. The network analyzer swept over a frequency range expected to include resonance. Due to variability in the devices, the resonant frequency could not be exactly predicted, nor could it be

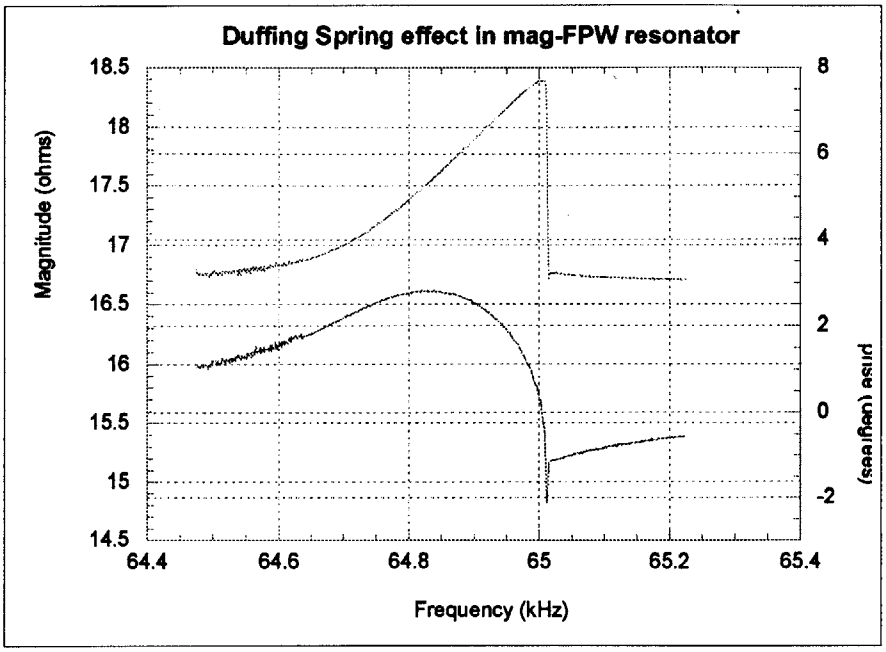

Figure 3 - Device response at high power

expected to be the same from one device to another. This is attributed to variations in the actual diameter of the membrane in the devices tested. The Bosch etch process in the lot 1 devices was not long enough to fully etch the opening beneath the membrane, and was followed by a wet etch intended to remove the remaining silicon. This however was done on a device-by-device basis because the etch of the silicon between adjacent dies had caused some of them to separate from the wafer during the Bosch process. As a result, devices fabricated in this way cannot be depended on to be uniform in diameter. In later lots, not analyzed here, the Bosch etch was carried out longer to improve removal of the silicon from beneath the membrane, but this resulted in the centers of some membranes being etched, causing non-uniform thickness across the membrane. Fortunately, this variation in thickness also creates a variation in mass per unit area, and the two factors offset in calculations of resonant frequency, as will be seen later.

When the resonant frequency was located, the range of the analyzer sweep was reduced to increase resolution around that point. The analyzer calculates and displays the complex impedance resulting from the motion of the conducting transducer through the external magnetic field. When the device is driven at its resonant frequency, a sharp peak is observed in the magnitude and a zero crossing in the phase of the device response (figure 4). At the 2.5-5 kHz span at which these measurements were originally made, there is not enough resolution to gauge the quality factor of the response. However, the zero

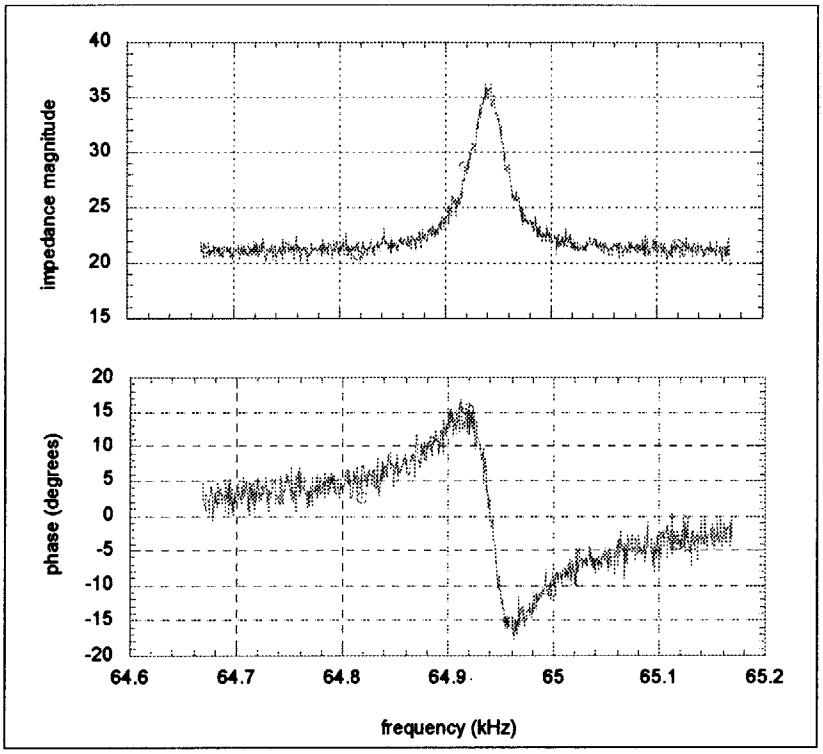

Figure 4 - Sample network analyzer output

crossing of the phase, and hence the resonant frequency, can be clearly tracked. The magnitude and phase of the response were recorded in data files for later analysis. Data sets were collected in this way for a number of environmental factors. Ambient gas was varied between air, argon, and helium, chosen to give a good cross section of gas

molecule size. A number of data sets were collected for each or these gases with the pressures varied over a range of 1 mT to 1 T. Above about 1 T, the signal to noise ratio became too small for the resonance to be accurately tracked.

2.2.3.2 Preliminary Analysis

Although the variability in diameter is a problem that must be corrected for eventual use as sensors, it is actually helpful in evaluating the behavior of the devices as it provides a greater range in one of the independent variables. The actual diameters of the devices were measured some time after the frequency measurements were made, and some of the tested devices could not be located. This is due to a variety of factors, including devices getting broken, mislabeled, or loaned out to other projects. More than one device were found with the same label, and it's likely that some of these correspond to the missing devices. Table 1 lists those devices for which both frequency and diameter are definitely known. On some devices, the diameter measured parallel to the transducer lines

Table 1 - Summary of tested devices

device	designed size (mm)	frequency (kHz)	diameter (mm)
In Argon			
fl152**	1	282	0.628
fl1a	1	228	0.854
fl1d	1	257	0.742
fl112*	2	127	1.765
fl166	2	123	1.521
fl155*	3	72	2.694
fl156*	3	64	2.750
In Helium			
fl153	3	65	2.700
fl152	3	57	2.685

* measured on a different instrument

** the device is mislabled

differed slightly from that measured transverse to those lines. In those cases, the diameter listed is the average of those two measurements. All of the devices listed were from the first wafer of lot 1, which completed the fabrication process first. Some devices from the second wafer of lot 1 were available later and tested in helium, but those that were tested couldn't later be located for measurement and aren't included in this part of the analysis. Devices from both wafers were used in the damping analysis later in this thesis. Both wafers were supplied to Sandia by MCNC with a 0.5 μm nitride layer already in place.

The range of diameters created allows for good direct comparison of diameter and

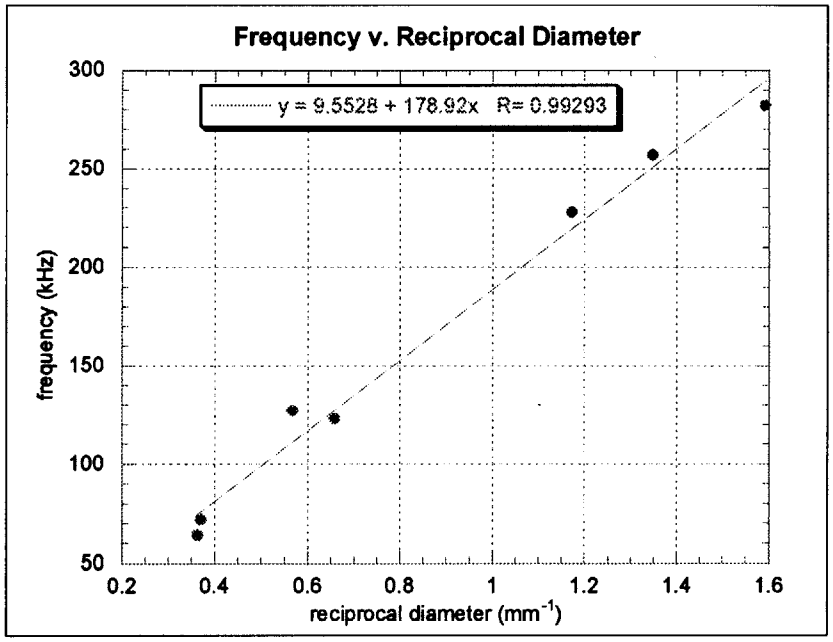

Figure 5 - Linear dependence of frequency on reciprocal diameter

frequency. A trend is visible in this data, which can be seen more clearly when the frequency is plotted against the reciprocal of diameter, as shown in figure 5. This linear relationship is consistent with the expression $\omega = \frac{1}{l}\sqrt{\frac{C_1 \sigma}{\rho}}$, where l is the diameter, ρ is mass density, and σ is the residual stress, from the energy method analysis of the circular membrane later in this paper. The constant C_1 depends on the membrane shape. The slope

of 178.92 khz•mm (m/s) gives a stress equal to $4\pi^2 \cdot 32012 \cdot \frac{\rho}{C_1}$. The actual density is not uniform, due to the placement of the aluminum transducer over the nitride disk. It can be modeled as $\rho_{eff} = \frac{t_n\rho_n + 0.54 t_a \rho_a}{t_n + t_a}$, where t_a and ρ_a are the thickness and density of the aluminum and t_n and ρ_n are the thickness and density of the nitride. The factor of 0.54 comes from the proportion of the nitride disk covered by the transducer. With typical values of 2700 kg/m^3 for aluminum and 2800 kg/m^3 for nitride, this gives an effective density of 2100 kg/m^3. For an ideal circular membrane, $C_1 = 4.0$, but for this data, that gives a stress of 632 MPa, which is much higher than the 140 MPa claimed by MCNC in their product specifications for the nitride coated wafers. One expects that the constant C_1 will be different for a device with such a complicated shape. The effective density approximation is also not completly accurate. A major goal of the model developed in this thesis will be to refine this analytic model to allow accurate prediction of the resonant behavior and to extract the actual stress in the devices tested.

3 Model

3.1 Circuit model

The ideal way to model a MEMS device so that it can be integrated into a circuit is as an electronic element. Such an element provides electrical terminals that interface with the mechanical features of the device and respond in the modeled circuit the same way the electrical terminals of the actual device do. In the case of the Lorentz force driven resonator in this thesis, the conversion between electrical and mechanical domains is achieved by a gyrator, which converts input current, a flow variable, to force, an effort variable, according to

$$\begin{pmatrix} F \\ \dot{x} \end{pmatrix} = \begin{pmatrix} 0 & n \\ \frac{1}{n} & 0 \end{pmatrix} \begin{pmatrix} v \\ i \end{pmatrix} \tag{1}$$

where $n = aB$, with a the total length of conductor moving in the magnetic field, B. The resonator itself is modeled first as a spring-mass system, shown in figure 6. The mass is

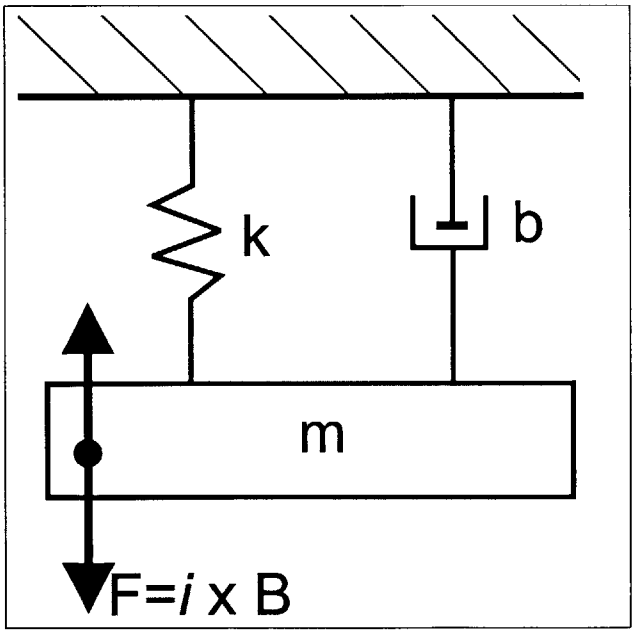

Figure 6 - Spring-mass system with Lorentz force drive

the effective mass of the device in the fundamental mode, the spring constant k is the stiffness of the membrane, and the dash-pot represents the damping due to the air or other fluid around the membrane. For small amplitudes, the spring is linear, $F=k \cdot x$, where k is the spring constant. At higher amplitudes, it exhibits Duffing spring behavior, described by $F = k\,(x + \varepsilon x^3)$, where ε is small. As a sensor, it is only used in the linear regime, though it will be useful to know at what amplitudes this model breaks down. The Lorentz force in this model is $i \times B$, integrated over the length of the transducer wires. Using the analogy that force is equivalent to voltage and velocity to current, the mechanical model becomes an RLC series circuit, with the dash-pot a resistor, the spring a capacitor, and the mass an inductor. The force is a source, or in this case the output of the gyrator. In addition, there is a resistor on the electrical side of the gyrator, representing the DC resistance of the electrode. The complete circuit is shown in figure 7. In practice, it is the

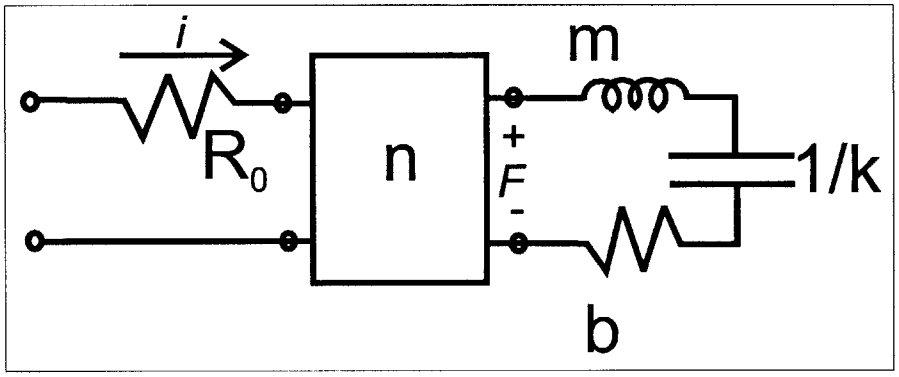

Figure 7 - Equivalent circuit representation

impedance of the device that is measured to find the resonant frequency. From this circuit, this electrical impedance can be found as a function of device and environmental properties.

On the mechanical side of the circuit, the impedance is described by

$$Z_m = \frac{F}{\dot{x}} = \frac{s^2 + \frac{b}{m}s + \frac{k}{m}}{\frac{1}{m}s} \tag{2}$$

Transfering this through the gyrator, the electrical impedance is

$$Z_e = R_O + \frac{n^2 \frac{1}{m}s}{s^2 + \frac{b}{m} + \frac{k}{m}} = \frac{R_O s^2 + \left(\frac{n^2}{m} + R_O \frac{b}{m}\right)s + R_O \frac{k}{m}}{s^2 + \frac{b}{m}s + \frac{k}{m}} \tag{3}$$

The value of R_0 depends on properties of the aluminum, wire bonding, and other external factors and is measured as part of device calibration. To find values of b, k, and m, we turn to mechanical modeling.

3.2 Analytic model

In mechanical design, a membrane is a plate in which the bending can be neglected and deformation is dominated by the stress in the material. The mechanical properties of a circular membrane are well studied and can be used to relate such things as stress, dimensions, deflection, and resonant frequency [10]. From these, we can find stiffness and effective mass. The fundamental-mode mag-FPW adds an unstudied level of complexity to the problem, with metal transducer lines crossing the top of the membrane. As a first level of approximation, the device can be regarded as a single membrane with a uniform density derived from the average density of the two materials. A more involved model could be made using a density function that varies with position in the plane. From the energy method solution of the membrane, distributed pressure is related to device characteristics according to:

$$P = \frac{C_1 \sigma_o t d}{l^2} + C_2 f(\nu)\left(\frac{E}{1-\nu}\right)\frac{t d^3}{l^4} \qquad (4)$$

Where P is applied pressure, C_1 and C_2 are constants, d is the deflection at the center of the membrane, t is the thickness, and l is the diameter. E is the Young's modulus and ν is the Poisson's ratio of the membrane [11]. For a circular membrane, $C_1 = 4.0$, $C_2 = 2.67$, and $f(\nu)=.957-.208\nu$. As mentioned above, these values may be different for the complicated structure of the mag-FPW.

The second term leads to nonlinear spring behavior and, under the assumption that the device is in fact linear, it can be neglected. Rewriting equation 1 in the form of Hooke's law, with $P=F/\pi l^2$, we have

$$F = \pi l^2 \cdot \frac{C_1 \sigma_o t}{l^2} \cdot d = C_1 \pi \sigma_o t \cdot d \qquad (5)$$

from which we obtain the effective spring constant $k_{eff}=C_1\pi\sigma_o t$. As long as the membrane approximation holds, this value is a constant arising from material properties. If the diameter to thickness ratio becomes such that bending has an effect on shape, it may change. From this and the effective mass, adjusted from actual mass by the factor C_m, we should be able to obtain the resonant frequency of the membrane:

$$\omega = \sqrt{\frac{C_1 \pi \sigma_o t}{C_m \rho \pi l^2 t}} = \frac{1}{l}\sqrt{\frac{C_1 \sigma_o}{C_m \rho}} \qquad (6)$$

The effective mass depends on actual mode shape and is found later in this chapter. Here we see that the frequency varies linearly with the reciprocal of diameter, as found in

the experimental data. From the slope of that line, we can determine the stress in the membrane, using finite element analysis to find values for the unknown constants.

Due to the complex design of the device, finding the actual values needed, taking into account the actual shape of the transducer and the difference in stress between the transducer wires and the membrane, would require a much more complicated analytical model. An alternative approach is finite element modeling, a very useful tool in the realm of MEMS devices.

3.3 Finite element model

3.3.1 Introduction

As more research is done on MEMS, it is becoming increasingly necessary to develop good tools for modeling these devices. Such tools will allow details of their operation to be examined without actually fabricating prototype devices, reducing the time and expense needed to develop new devices. As shown earlier, standard analytic solutions are inadequate for describing complicated MEMS structures. Tools such as Abaqus and Ansys, designed for modeling mechanical systems, prove useful for modeling the mechanical behavior of MEMS devices, though they can run into difficulty with the thin films and high aspect ratios present in MEMS.

3.3.2 Memcad

One powerful tool for MEMS modeling is Memcad, developed at MIT and now marketed by Microcosm of Cambridge, MA. Memcad brings together tools for process simulation and finite element model analysis. It allows researchers to investigate mechanical, thermal, electrostatic, and other interesting properties of their designs and automates many of the tasks associated with this sort of modeling.

3.3.3 Fabrication process

To create my model in Memcad I began with the actual process used to fabricate the devices, summarized in Appendix A. After importing the mask files from Sandia and modifying them to work with the CIF format used by Memcad, I defined a process flow in Memcad that would simulate the actual process. Due to the requirement in Memcad that every deposition be associated with an etch, I had to add some steps, such as etching the nitride. The MemBuilder component used this info to create an accurate solid model of the device in I-Deas with an extra sacrificial layer of oxide and base layer of silicon that were simply put away and ignored for the rest of the simulation. The release etch of a normal MEMS device is accomplished in MemBuilder by "putting away" the sacrificial layer, which doesn't exist in the mag-FPW. Table 2 shows the process flow from Memcad's process editor. The real steps are the deposition of nitride and aluminum on top, etching that aluminum, and the etching of the silicon from the backside. The extra steps are the deposition of the silicon and the deposition, etch, and removal of sacrificial oxide. The real steps of depositing and later etching nitride on the backside are left out, since that nitride

Table 2 - Process steps in Memcad's device creation component

step	action	material	thickness	mask
0	Base	Silicon	1000	
1	Deposit	Crystal Silicon	500	
2	Etch	Crystal Silicon		L3
3	Deposit	SiN	0.5	
4	Etch	SiN		L2
5	Deposit	Aluminum	0.55	
6	Etch	Aluminum		L4
7	Deposit	Oxide	1	
8	Etch	Oxide		L2
9	Sacrifice	Oxide		

doesn't have any bearing on the operation of the final device and would just add time and complexity to the MemBuilder process.

3.3.4 Meshing the model

The solid model produced by MemBuilder was not quite ready for meshing, due to the complexity of the device's design. As created, the membrane was modeled as a single square layer covering the entire die, and the transducer a large spiral with no subdivisions. Since only the moving parts need to be meshed, i.e., the portion of the membrane and transducer over the hole in the silicon, it was necessary to create partitions in these parts so that I-Deas would regard them as separate from the nonmoving sections of the structure. Additionally, to allow finite element nodes in the transducer and membrane to

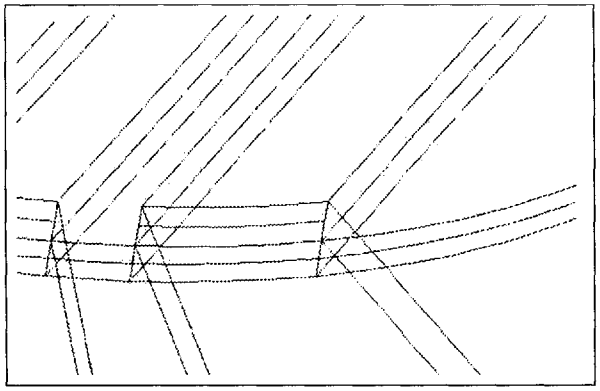

Figure 8 - Partition to allow meshing only of moving parts

align, I partitioned the membrane into 13 sections according to where it came into contact with the transducer (Figure 8). Due to the extreme aspect ratio of the device, it was necessary to scale it by a factor of 100 in the z (normal to the membrane) direction to allow accurate meshing in I-Deas, which seems to have some difficulty with extremely thin structures. To assure proper interaction between the transducer and membrane, it was necessary to join the two parts so that a single finite element model could describe both.

After preparing the model, I generated a surface mesh of parabolic (3 nodes per edge) quadrilaterals approximately 70 μm square on the top surfaces of both materials. This was a mapped mesh in the nearly rectangular transducer sections and inner partitions of the nitride layer. I used a free mesh in the two outer sections that exhibit the most curvature, with the desired edge length set to make the nodes align with those of the adjacent mapped meshes. I then extruded these meshes through the thicknesses of their respective parts creating parabolic brick elements. I chose the size to keep the mesh simple while avoiding sharp angles in the deformed elements at the corners where the transducer lines meet the edge of the circle as shown in figure 9. It would be ideal to have the elements as small as possible, thereby reducing both the angles and the aspect ratio that will exist after scaling the device back to its proper thickness. Unfortunately, making the mesh elements smaller greatly increases the size of the model and strains the capabilities of

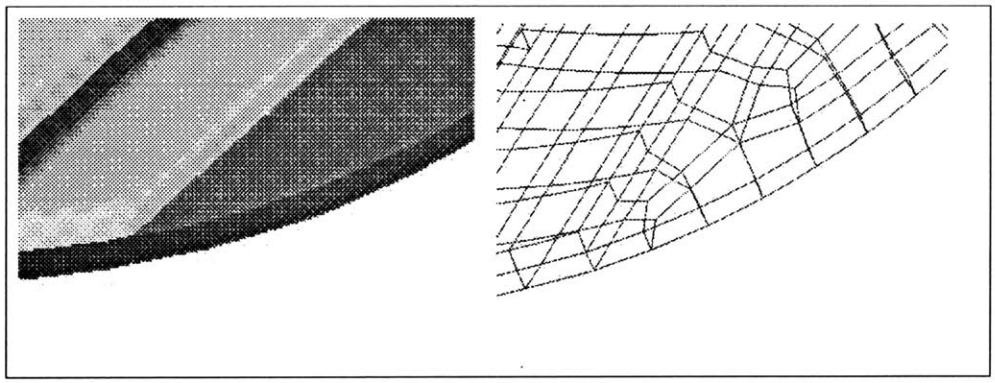

Figure 9 - The different surfaces of the solid model and the mesh used to model them

the computer. This size seemed to work adequately, producing reasonable results in acceptable amounts of processing time. After joining the coincident nodes that result at the intersection of the two meshes and removing the original shell elements, I exported this mesh into the file format that Memcad uses as input.

3.3.5 Verification

To verify that the model would work, I used the MemMech tool in Memcad to find the first three modes of this meshed structure, applying the boundary condition that the rim of the membrane disk is fixed in all degrees of freedom. Though only the first mode is expected in these structures, due to the uniform direction of the excitation force, it is generally advisable to model two modes higher than needed to assure accuracy through the desired mode. The program produced the correct circular mode shapes, though of course the actual deflections and frequencies were of little use due to the scaling of the device in the z axis. To remove this scaling and examine other properties of the device, I turned to the SimMan component of Memcad. SimMan allows the user to specify up to three trajectories which can be discrete values, steps, or other functions. In each repetition, the corresponding values from each trajectory can be used to scale any component of the model such as dimension, material property, or loads. I defined the first trajectory to create a scaling of 0.01 in the z direction to undo the scaling that had been necessary for proper meshing in I-Deas. This produced frequencies and deflections that were within the range of the observed behavior of the devices. I then used the second trajectory to scale the diameter of the device, since all three sizes of device are simply scaled versions of each other. This left one trajectory for examination of other material properties and environmental conditions to observe their effects on the behavior of the

device. The mode shapes generated by the model are shown in figure 10 with the deflection greatly exaggerated.

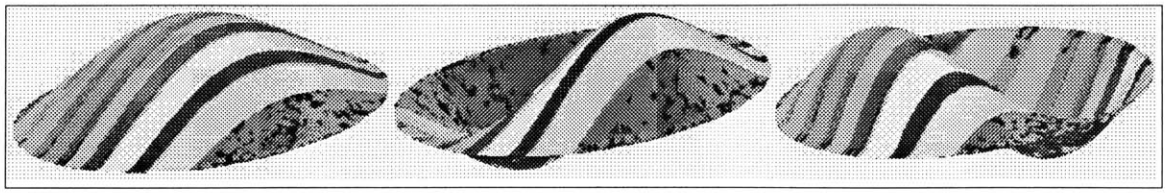

Figure 10 - The first three modes computed in Memcad, vertically exaggerated

3.3.6 Simulations

3.3.6.1 Overview

The material properties and environmental conditions of greatest interest, due to their effects on the behavior of the device, uncertainty in their value, and their relationship to mechanical values needed for the circuit model, are residual stress in the nitride and in the aluminum, the density of the nitride and the aluminum, and the resulting effective stress and density of the device. Also of interest are the effects of ambient temperature and pressure. I used the Memcad model to investigate the effects of these properties on the behavior of the device and compared these results to the actual data. These comparisons allowed for improvement of the analytic model and agreement between both models and the observed data, and subsequently values for the mechanical constants in the circuit mode.

3.3.6.2 Residual Stress

As shown by equations 5 and 6, the residual stress in the silicon nitride and in the aluminum is expected to be the parameter most affecting frequency and deflection, dimension and density being fixed. Resonant frequency will vary with the square root of the effective stress in the device. As was shown by the data, knowing what value to use

for the effective stress in the structure is critical to finding values that will allow the use of the other models to accurately predict resonant frequency from the device design.

The researchers at Sandia who fabricated the devices originally thought that the aluminum was stress free, but later found evidence that there may be compressive stress in some lots of devices [12]. To examine these possibilities I ran multiple simulations, setting the stress in either the aluminum or the nitride to expected values and varying the other. The manufacturer of the nitride, MCNC, reported that its residual stress was below 140 MPa. This value however resulted in much lower resonant frequencies in the model than were observed in the devices. To see if the aluminum could account for this discrepancy, I examined the effects of increasing compressive and tensile stress in the aluminum, but found that it would have to be tensile stress well above the maximum reported yield strength of 124 MPa to raise the resonant frequency to observed levels [13]. Additionally, I found that the relationship between the slope of frequency versus reciprocal diameter and the stress in the aluminum was nearly linear, implying that it is not the dominant factor in the effective stress of equation 6. Assuming then that the actual stress in the silicon nitride was higher than expected, and that this was the dominant stress in the structure, I set the stress in the aluminum to zero and explored what values of residual stress in the nitride would result in frequencies near what was observed.

Using the SimMan tool in Memcad, I defined a simulation that would find the resonant frequencies for each of the actual diameters for which data was available as described in section 2. I ran this simulation using nitride stress values of 300, 400, and 500 MPa, the range which in some preliminary simulations gave frequencies closer to those observed than did the expected 100 MPa. The slope of frequency versus reciprocal

diameter should vary according to $\frac{f}{1/l} = C\sqrt{\sigma}$, from equation 6, where the constant $C = \frac{1}{2\pi}\sqrt{\frac{C_1}{C_m \rho}}$. Figure 11 plots the calculated slope against the root of the simulated stress, showing the expected linear dependence. From the line fit to these points the value of C is found to be 1.057×10^{-2} $m \cdot s^{-1} Pa^{-1/2}$. Using this and the 178.92 $m \cdot s^{-1}$ slope of the experimental data, stress is found to be 336 MPa.

To verify that the effective stress of the resonator was dominated by the stress in the nitride and not by that in the aluminum, I fixed the nitride stress at 336 MPa and found

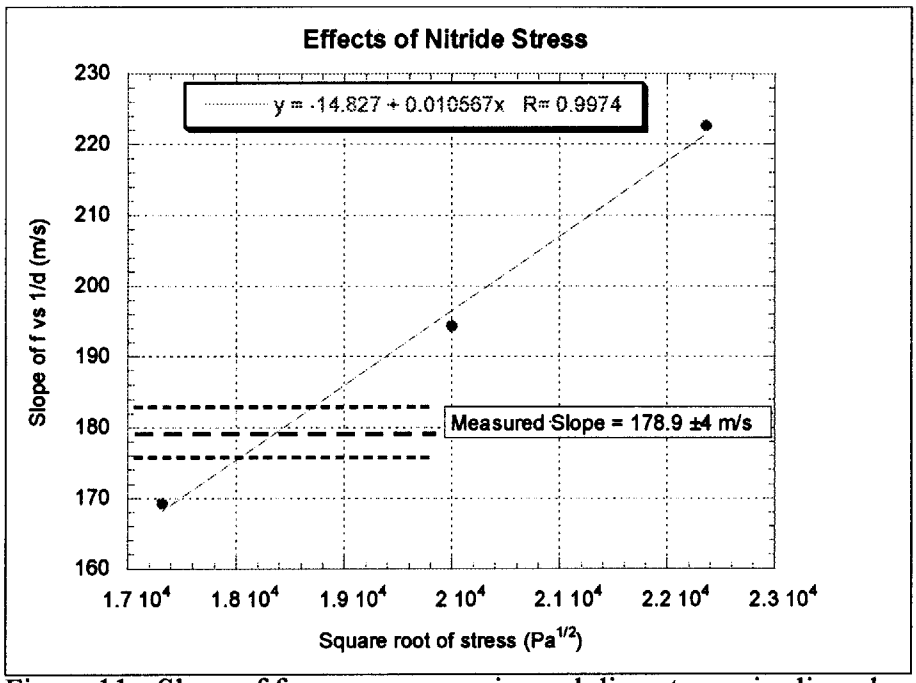

Figure 11 - Slope of frequency vs. reciprocal diameter varies linearly with square root of nitride stress. (Al stress = 0)

the slope of frequency versus reciprocal diameter over a range of tensile and compressive aluminum stress values. With the stress in the aluminum varying from 50 MPa compressive to 50 MPa tensile, the slope of frequency versus reciprocal diameter varied linearly with stress (figure 12), verifying that it is not the dominant stress, though it does

have some effect. Its effects are large enough that they must be considered in device and process design, but not enough to allow extraction of its value from the available data, given the many other uncertainties.

In addition to stresses in both materials, other uncertainties include the unknown

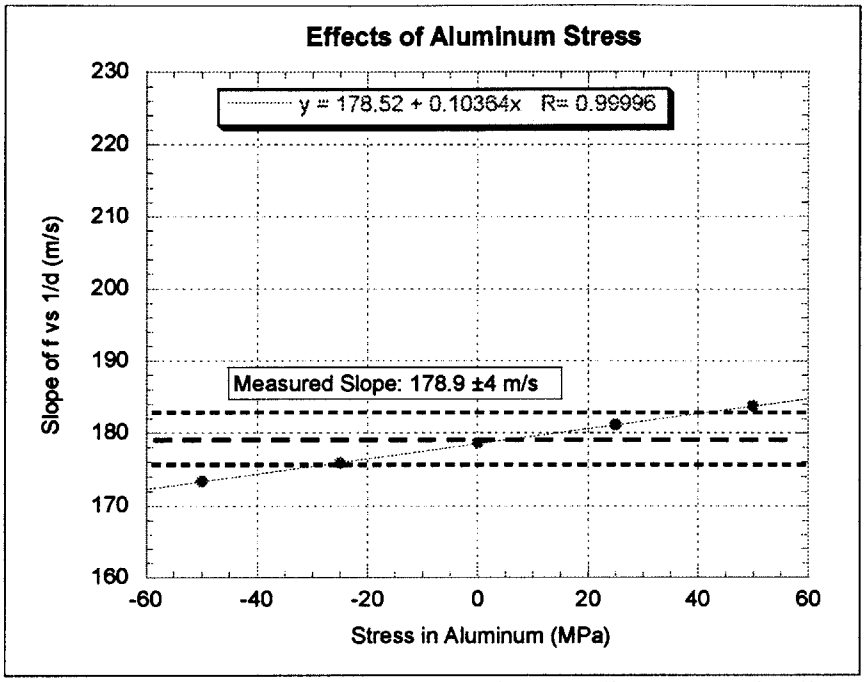

Figure 12 - Slope of frequency vs. reciprocal diameter varies linearly with aluminum stress (SiN stress = 336 MPa)

densities of the materials and the changing effect of the transducer on membranes of different size. Since the model scaled the transducer to match the diameters of the under-etched holes in the silicon, it is not as accurate as it could be. To allow scaling of the hole independently of the transducer would require either a significantly more complex finite element model or a different model for each device, representing its actual dimensions. This is a problem that will be eliminated by a more controlled process resulting in uniform devices, as would be required for actual use of this device as a sensor.

3.3.7 Analysis

After finding the stress value in the silicon nitride and making the finite element model produce the correct frequencies for the known diameters, the model can be used to find the mechanical circuit parameters needed. In addition to frequency and deflection for each mode, the Memcad results include the effective mass of the resonator. This mass is the effective mass that must be used in the expression $\omega = \sqrt{\frac{k}{m}}$, reflecting the fact that the membrane mass is not moving uniformly up and down, but is deflected according to radial position. From this mass and the resonant frequency, the stiffness, $1/k$, can be found. I configured SimMan to use the effective stress found above and to examine ten diameters evenly spaced over the range 0.5 mm to 3 mm. From the frequency and mode mass computed by the model, I computed a value for k of 489.5 Nm^{-1} (figure 13). I noted however that the lowest point, 0.5 mm diameter, was not near the others. I then computed results for diameters from 0.1 to 0.7 mm, spaced more finely than before, to see why this

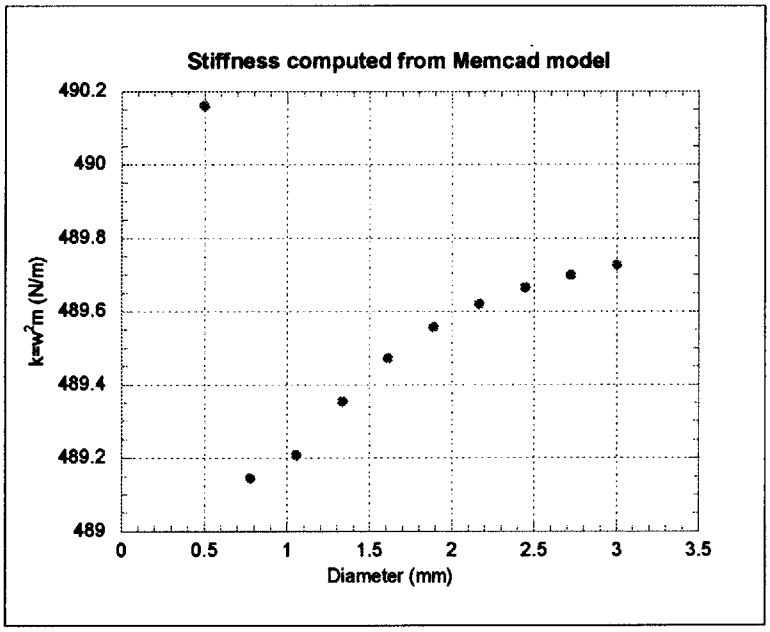

Figure 13 - The k value computed from the Memcad model is relatively constant above d=0.6 mm

point was out of place. The k computed from these results show that it is generally constant but decreases slightly for diameters below 1 mm and then increases dramatically for diameters below roughly 0.6 mm. This result is consistent with values extrapolated for f and m over this range, and indicates a minimum size for such a device that will work with this model. Below that size, the bending effects near the edge of the membrane affect a sufficiently large proportion of the membrane to not be neglected.

From the value of k computed and the slope, s, of the frequency versus reciprocal diameter, effective mass can be found directly from diameter and these constants as follows:

$$s = \frac{f}{1/l} = \frac{\omega l}{2\pi} = \frac{l}{2\pi}\sqrt{\frac{k}{m}} \tag{7}$$

$$m = \frac{kl^2}{4\pi^2 s^2} \tag{8}$$

The one remaining value to be found is b, the damping constant. This depends on the viscosity of the air around the resonator and can be found from the dimensions of a device and the quality factor of a particular response according to

$$b = \frac{\sqrt{km}}{Q} = \frac{kl}{2\pi s Q} \tag{9}$$

where Q is the root 2 bandwidth over frequency. Alternatively, it can be found from the

maximum impedance at resonance, Z_r, since the second and zero order terms of the transfer function can be neglected, leaving

$$Zr = \frac{\left(\frac{n^2}{m}+R\frac{b}{m}\right)}{\frac{b}{m}} = \frac{n^2+Rb}{b}; b = \frac{n^2}{Z_r-R} \tag{10}$$

Having found these values, the next step is to verify that the transfer function for the equivalent circuit produces the proper response and use it to find damping values for the various gasses and pressures examined. A simple script in Matlab shows that this transfer function produces the correct shape response when using the calculated values for k and m and a value for b computed as in equation 10. It takes as input the resonant frequency, DC impedance, and maximum impedance. It also reads in the experimental data so that it can be plotted against the model for comparison (figure 14), and returns the damping value it used and the diameter computed from the resonant frequency. Since the

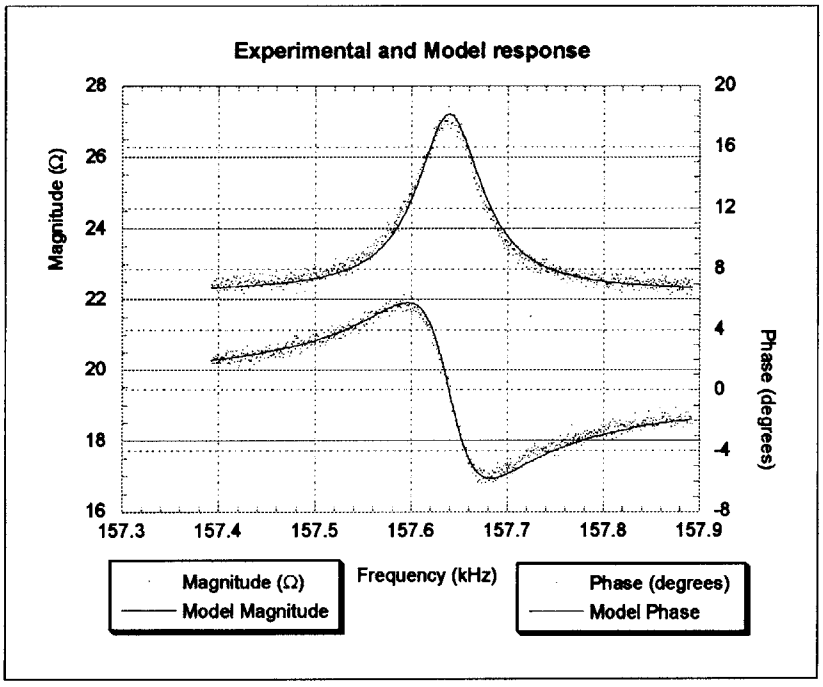

Figure 14 - Experimental and Circuit Model response

devices on which damping data is available couldn't be found for diameter measurements, the program computes the diameters from the resonant frequency. The width of the resonant peak varies with magnetic field strength, and five of the six sets of damping data required a field strength of 0.18 T for optimal fit. The sixth set, a 3 mm device in air, required a lower field of 0.14 T to fit. These are lower than the measured value of 0.25 T, measured with a digital magnetometer. Table 3 summarizes the damping values found through this process. As expected, damping increases with increasing pressure and with size. Plotting damping divided by area, as a function of pressure, the damping in air appears to have a similar linear dependence for all three tested devices (figure 15), while the helium data is too noisy to quantify the dependence (figure 16).

Table 3 - Damping factor *b* computed from circuit model

	Air			Helium		
	nominal diameter (mm)					
	1	2	3	1	2	3
Pressure	*computed diameter (mm)*					
(MPa)	1.135	2.739	2.762	1.091	2.755	2.816795
50	9.30E-08	4.247E-07	5.810E-07	6.706E-08	2.925E-07	1.3742E-06
100	1.31E-07	6.082E-07	6.864E-07	5.122E-08	3.576E-07	1.4254E-06
200	1.70E-07	8.305E-07	8.787E-07	1.070E-07	4.881E-07	1.4523E-06
300	2.11E-07	1.021E-06	1.046E-06	1.219E-07	5.687E-07	1.6776E-06
400	2.45E-07	1.172E-06	1.270E-06	1.334E-07	6.753E-07	2.0393E-06
500				1.491E-07	7.016E-07	1.8857E-06
600	3.07E-07	1.522E-06	1.665E-06	1.531E-07	7.449E-07	1.6756E-06
700				1.552E-07	8.209E-07	1.8844E-06
800	3.61E-07		2.198E-06	1.666E-07	8.501E-07	1.9319E-06
900				1.691E-07	8.917E-07	1.8828E-06
1000	4.24E-07		2.443E-06	1.799E-07	9.629E-07	2.0352E-06
1100				1.921E-07	1.047E-06	2.0910E-06
1200	4.56E-07		2.748E-06	1.888E-07	1.047E-06	2.3516E-06
1300				1.954E-07	1.146E-06	2.3510E-06
1400	4.92E-07		3.097E-06	1.921E-07	1.147E-06	2.4257E-06

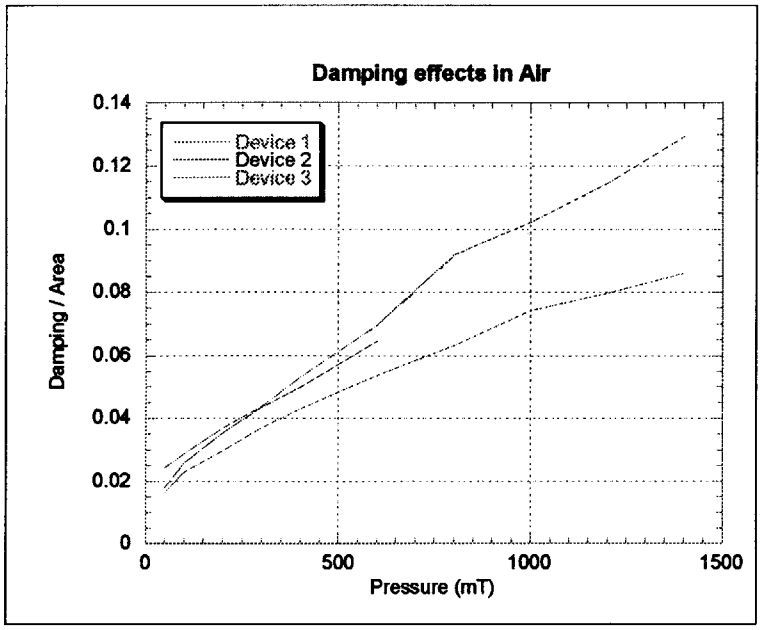

Figure 15 - Damping in air varies linearly with pressure

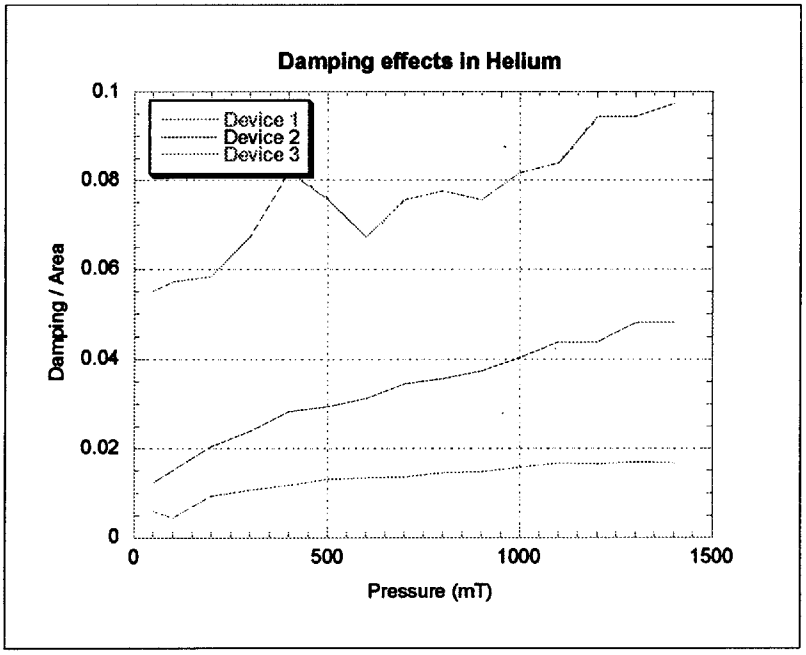

Figure 16 - Damping in Helium is too noisy for conclusions

4 Conclusions

4.1 Models & Data

4.1.1 Lumped Element Model

This thesis has demonstrated that a lumped element model, interpreted as an equivalent circuit, can accurately describe the behavior of the fundamental-mode mag-FPW. Values and functional dependencies were found for the model parameters of stiffness, mass, and damping. These values were used to show that the equivalent circuit representation will generate the same frequency response that was observed in the actual devices. This circuit model will allow a circuit designer to integrate the device into whatever control electronics they like, relieving them of the need to deal with mechanical representations of the device. It also indicates limits on the device size at which the linear model breaks down and makes the device more complicated and less useful. By defining the circuit element parameters k, m, and b as functions of diameter and providing a clear relationship between diameter and resonant frequency, the model allows existing devices to be quickly characterized and calibrated. The damping value b was found for the range of tested pressures and to some extent follows expected patterns, though more data is needed to assure accuracy in this part of the model.

4.1.2 Finite Element Model

The finite element model created in this thesis demonstrates that tools such as Memcad are effective for modeling MEMS devices. In addition to demonstrating that such models accurately describe device behavior, it allows the extraction of material properties of existing devices and mechanical values needed for the circuit model. The residual stress in the silicon nitride was found to be higher than intended, and it was demonstrated that

this was the dominant stress in determining device performance. These results can be used to find the stress in future lots of the modeled devices without difficulty. Stress in the aluminum was found to not be a significant factor in device performance. The finite element model provided frequency and mode mass parameters needed to find a value for stiffness and showed that this value is valid for all tested diameters. The model also shows that the unexpected variations in resonant frequency between devices can be explained by variations in membrane diameter resulting from process non-uniformity.

4.2 Future Work

There are several ways to improve upon the current model. As mentioned above, a more complicated finite element model that allows independent scaling of the transducer and membrane would be an improvement, though with the current tools it would be a harder model to create and use. In addition to compensating for the current non-uniformity in device size, it would allow easier incorporation of changes such as the thickness of the membrane or transducer. It also may improve the model to use shell mesh elements rather than brick, though this is currently a limitation of the Memcad tool. That would improve computation time by significantly reducing the total number of nodes in the mesh. Fewer nodes per mesh element would also allow more elements, making them smaller and reducing sharp angles. Characterization and calibration of actual devices can be improved through the use of on-chip structures, such as the M-test, to allow more direct measurement of mechanical material properties. This would allow the model to directly produce the needed lumped element values without first testing devices and then using the model to find values for these material properties.

References

1. D.S. Ballentine, S.J. Martin, A.J. Ricco, G.C. Frye, D.J. Ballentine, *Acoustic Wave Sensors : Theory, Design, and Physico-Chemical Applications*, Academic Press, Boston, 1996.

2. S.W. Wenzel and R.M. White, "Silicon-based ultrasonic Lamb-wave multisensors," *Solid-State Sensor and Actuator Workshop Technical Digest*, IEEE, 27 -30, 1988.

3. S.W. Wenzel and R.M. White, "Flexural plate-wave sensor: chemical vapor sensing and electrostrictive excitation," *Proc.Ultrasonics Symp.*, vol.1 pp. 595 -598, IEEE, 1989.

4. B.J. Costello, B.A. Martin, and R.M. White, "Acoustic plate-wave biosensing," Engineering in Medicine and Biology Society,. *Images of the Twenty-First Century., Proceedings of the Annual International Conference of the IEEE* , vol.4, pp. 1108-1109, IEEE, 1989.

5. C.E. Bradley and R.M. White, "Acoustically driven flow in flexural plate wave devices: theory and experiment," *Proc.Ultrasonics Symp.*, vol.1, pp. 593 -597, IEEE, 1994.

6. S.J. Martin, M.A. Butler, J.J. Spates, W.K. Schubert, and M.A. Mitchell, "Magnetically-excited flexural plate wave resonator," *Proc. Intl. Frequency Control Symposium*, pp. 25-31, IEEE, 1997.

7. M.A. Butler, M.K. Hill, J.J. Spates and S.J. Martin, "Pressure sensing with a flexural plate wave resonator," *J. App. Physics*, vol. 85 no. 3, pp. 1998-2000, AIP, 1998.

8. W.K. Schubert, personal communication 8/98

9. W.K. Schubert, personal communication 3/99

10. S. Timoshenko and S. Woinowsky-Krieger, *Theory of Plates and Shells*, 2nd ed., McGraw-Hill, 1959.

11. S.D. Senturia and M.A. Schmidt, "Notes on material properties," *Microsystems: Mechanical, Chemical, Optical*, pp. 9.22-9.23, MIT, 1997.

12. W.K. Schubert, personal communication 2/99

13. D.T. Read and J.W. Dally, "Mechanical Behavior of Aluminum and Copper Thin Films," *Mechanics and Materials for Electronic Packaging: Volume 2, Thermal and Mechanical Behavior and Modeling*, ed. by M. Schen, H. Abe, and E. Suhir, American Society of Mechanical Engineers, AMD-Vol, 1994, via *http://mems.isi.edu/mems/materials/measurements.cgi?MATTAG=aluminumalfilm*

Appendix A - Fabrication Process of Sandia National Laboratories' Magneticalley-excited Flexural Plate Wave Resonator

Process

The fabrication of the fundamental-mode mag-FPW is fairly simple, involving only two masks. The wafers were provided to Sandia with the silicon-nitride layer already deposited. Aluminum was deposited on the top surface and etched with the first mask to create the transducer. The nitride on the back was then patterned with the second mask but the photoresist used for that etch wasn't removed. The front was then coated with a protective layer of photoresist to shield the aluminum and the nitride from the next step. Finally, the Bosch etch process was used to create a hole entirely through the wafer, leaving only the nitride on the front side with the patterned aluminum transducer on it. In the first lot of devices, the Bosch etch wasn't carried out long enough to completely open the circular hole beneath the membrane, leaving a small "foot" of silicon. This was removed with a wet etch to clear the hole. Because the Bosch etch separated the individual devices, this final etch was not uniform and nominally identical devices may vary in diameter. In the second lot, the Bosch etch was carried out longer, completely opening the holes, but in some cases it etched into the membrane, resulting in non-uniform thickness.

The attached runsheets, courtesy of Kent Schubert as Sandia, provide the details of the process, including chemicals used and time of exposures and etches.

Lot 1 (devices f1-1-x-x and f1-2-x-x) runsheet

Step	Process	Wafers	Description	Comments	Processing Notes
1	Label	1-2	Technet wafers with 0.5 micon LSN		W1-2 from Technet wafers w/ 5000 A low stress nitride on <100>, n-type, 4 in. Si, dated 4/25/97
2	Piranha clean	1-2	preparation for metal deposition		5 min clean on each wafer.
3	Al deposition	1-2	fronts 5500 A		5005 A Al dep in e-beam system; stopped after 500 A because rate fell to 0, crucible appeared OK, continued with additional 5000 A at higher power. Dektak thickness 4266 A
4	HMDS	1-2	fronts		coated w/ HMDS @ 5 KRPM for 30 s immediately prior to PR application
5	PR coat	1-2	fronts		coated w/ AZP 4620 @ 5 KRPM for 30 s, 10 m 85 C softbake.
6	PR exposure	1-2	fronts, FUND FPW98A METAL LAYER mask, 5" plate for 4" wafers, use MA 6 in CSRL aligner		exposed W1 -2 for 8 sec on MA6 w/ soft contact & 30 micron exposure gap.
7	PR develop	1-2			developed in AZ 400K 1:4 prediluted for W1-1 m, W2-1.5 m, hardbaked 10 m 110 C.
8	Metal etch	1-2	use Al etchant		etched W1-3.75 m, W2-4.0m in Al etch solution of 500 ml H20, 10 g K2Fe3(CN)6, 1 g KOH.
9	Solvent PR strip/clean	1-2			
10	HMDS	1-2	backs		
11	PR coat	1-2	backs		
12	PR exposure	1-2	backs, FUND FPW98A BOSCH MEMBRANE mask, align to the metal targets on the front side		
13	PR develop	1-2			
14	Nitride etch	1-2	backs, 790 RIE in CSRL		
15	Bosch etch	1-2	backs, until clear through - wafers are about 400 microns thick	Be sure Christi and Randy know this is for the NEP/EFI project (Case # 7445.100)	for front side protection during Bosch etch, coated w/ AZP4303 A 4 K RPM, no softbake to prevent re-flow of patterned PR, dried overnite.
					Etched Si foot 3:5:3 HF:HNO3:CH3CO2H to clear past Al lines

Lot 2 (devices f2-x-x-x) runsheet

Step	Process	Wafers	Description	Comments	Processing Notes
1	Label	1-4	W1,2 - Strataglas SSP with 1-um nitride. W3,4 - Stanford 2-um nitride on SSP wafers		
2	Piranha clean	1-4	preparation for metal deposition		
3	Al deposition	1-4	fronts 5500 A		Deposited 5505 A total Al in 2 runs, 3000 A, ther additional 2500 A.
4	PR coat	1-4	fronts		Coated w/ AZ 4110 @ 5 K RPM for 30 s, 90 s 9 C hotplate softbake.
5	PR exposure	1-4	fronts, FUND FPW98A METAL LAYER mask, 5" plate for 4" wafers, use MA 6 in CSRL aligner		Exposure time 4 s, vacuum contact
6	PR develop	1-4			Develop time 1 m 20 s in 1:1.4 312 developer
7	Metal etch	1-4	use Al etchant		Etched for 3-5 m in Al etch until metal cleared.
8	Solvent PR strip/clean	1-4			AZ 4330 on fronts didn't strip in acetone, ran 30 UV/ozone clean on backs.
9	PR coat	1-4	fronts	AZ4330 @ 4 K RPM, 90 C 5 m softbake	
10	PR coat	1-4	backs	AZ 4903 @ 2.5 K RPM, 120 C 5m softbake	
11	PR hydration	1-4		Leave in CSRL PR bay overnite to fully hydrate PR	
12	Edgebead exposure	1-4	backs	Exp. time 2 m	ommited per Christ W., will not be using 4" carri in Bosch etch system, so is not necessary. Exposed on MA6 in vacuum contact
13	Edgebead develop	1-4		AZ 400K 1:3 developer, 3 m	ommited per Christ W.
14	PR exposure	1-4	backs	FUND FPW98A BOSCH MEMBRANE mask, align to the metal targets on the front side, exp time 35 s.	Exposed on MA6 in vacuum contact
15	PR develop	1-4		AZ 400K 1:3 developer, 3 m	Numerous PR defects in field, PR appears to ha adhered to mask while in contact and been torn, open to SIN layer. Will rework from step 8.
16	Flood expose	1-4	backs	Exp. time 2 m	
17	Nitride etch	1-4	backs, Vacutek or 790 RIE in CSRL		
18	Bosch etch	1-4	backs, until clear through - wafers are about 525		